Immune modulation by helminths and the impact on the development of type 2 diabetes

Ruiter, K. de

4

THE *SCHISTOSOMA MANSONI* GLYCOPROTEIN OMEGA-1 IMPROVES WHOLE-BODY METABOLIC HOMEOSTASIS INDEPENDENT OF ITS TH2 POLARIZING CAPACITY

Hendrik J.P. van der Zande, Karin de Ruiter, Michael Gonzalez, Ruud Wilbers, Mariska van Huizen, Kim van Noort, Frank Otto, Cornelis H. Hokke, Arjen Schots, P'ng Loke, Maria Yazdanbakhsh and Bruno Guigas

Thesis Chapter

ABSTRACT

Type 2 immunity is involved in the maintenance of metabolic homeostasis and its disruption during obesity promotes chronic low-grade inflammation. Helminth parasites are the strongest natural inducers of type 2 immunity and we previously reported that infection with *Schistosoma mansoni* or treatment with a mixture of soluble egg antigens (SEA) both improved whole-body metabolic homeostasis in insulin-resistant obese mice. In the present study, we investigated the effects of two plant-produced glycosylation variants of omega-1, a glycoprotein present in SEA that has been shown to trigger dendritic cell-mediated Th2 polarization by a glycan-dependent mechanism, on whole-body metabolic homeostasis. We showed that both recombinant omega-1 glycovariants decreased fat mass and improved whole-body metabolic homeostasis in obese mice, an effect associated with increased adipose tissue Th2 cells, eosinophils and alternatively-activated macrophages. In the liver, omega-1 did not affect hepatic steatosis but increased IL-13-expressing Th2 cells and expression of fibrotic gene markers. Remarkably, the metabolic effects of omega-1 were still observed in obese STAT6-/- mice, although the Th2-mediated immune response was completely abolished. Omega-1 did not affect locomotor activity or energy expenditure but inhibited food intake in both WT and STAT6-/- mice. Altogether, we conclude that the improvement of metabolic homeostasis by omega-1 is independent of its Th2-inducing capacity and may be explained by brain-mediated inhibition of food intake and/or immune-independent direct interaction of omega-1 with metabolic cells.

INTRODUCTION

Obesity is associated with chronic low-grade inflammation in metabolic tissues (1). This so-called meta-inflammation plays a prominent role in the etiology of insulin resistance and type 2 diabetes (1-4), and is notably associated with increased numbers of pro-inflammatory macrophages in white adipose tissue (WAT) (5), liver (6, 7) and skeletal muscle (8, 9). In WAT, these macrophages mainly originate from newly-recruited blood monocytes that differentiate into pro-inflammatory, classically-activated macrophages (CAMs) upon entering the inflammatory milieu (5) and/or being activated by elevated local concentration of free fatty acids (10). These pro-inflammatory macrophages produce cytokines, such as tumor necrosis factor alpha (TNF-α) and interleukin 1-beta (IL-1β), which directly inhibit canonical insulin signaling (as reviewed in (2)) and contribute to tissue-specific insulin resistance and whole-body metabolic dysfunction. In the liver, activation of Kupffer cells, the resident macrophages (11), promote the recruitment of pro-inflammatory monocytes (6) and neutrophils (12) which trigger hepatic inflammation and insulin resistance through the production of pro-inflammatory cytokines and elastase, respectively (6, 11-13). While obese adipose tissue is thus characterized by pro-inflammatory type 1 cytokines, a type 2 cytokine environment is present in metabolic tissues under homeostatic, insulin sensitive conditions. Indeed, type 2 innate lymphoid cells (ILC2s) and T helper 2 (Th2) cells produce the type 2 cytokines IL-4, IL-5 and IL-13 in healthy adipose tissue and sustain a WAT eosinophils and alternatively activated macrophages (AAM) axis that is largely driven by eosinophil-produced IL-4 (14, 15). According to the current paradigm, AAMs are the final effector cells of this type 2 immune response that sustain insulin sensitivity through underlying molecular mechanism(s) that are still largely unknown.

Parasitic helminths are the strongest natural inducers of type 2 immunity (16). Interestingly, soil-transmitted helminth infection was reported to be associated with higher insulin sensitivity in humans (17), suggesting that helminth-induced type 2 immunity could protect against metabolic disorders. Moreover, both the short-lived rodent helminth *Nippostrongylus brasiliensis* and human *Schistosoma mansoni* improved insulin sensitivity and glucose tolerance in high-fat diet (HFD)-induced obese mice, an effect associated with strong WAT eosinophilia (15, 18). We also showed that chronic treatment with *S. mansoni* soluble egg antigens (SEA) promoted eosinophilia, T-helper 2 cells (Th2), type 2 cytokines expression and AAMs in WAT, and improved whole-body metabolic homeostasis (18).

SEA drives DC-mediated Th2 skewing at least partly through glycosylated molecules ((19), and reviewed in (20)). More specifically, an unknown Dectin-1/2-ligand in SEA (21, 22) and the T2 RNAse glycoprotein omega-1 (ω1; (23, 24)) have been shown to drive Th2 skewing. We have previously reported that ω1 is internalized by human DCs through an interaction between its glycans and the mannose receptor, and promotes Th2 skewing through interfering with protein synthesis (24). Interestingly, acute treatment of HFD-fed obese mice with human embryonic kidney 293 (HEK-293)-produced recombinant ω1 was recently shown to decrease body weight and improve whole-body glucose tolerance

through an IL-33-ILC2-axis (25). In this study, the metabolic effect of ω1 was reported to be glycan-dependent, yet we have previously shown that glycans on HEK-293-produced ω1 differ significantly from *S. mansoni* native ω1 (23, 24). Notably, HEK-293-produced ω1 glycans did not express the immunogenic Lewis-X (Le^X) motifs present on native ω1, but rather expressed LDN-F (24), a glycan motif with similar C-type lectin-binding properties as Le^X. However, as *S. mansoni* expresses an abundance of complex and unique glycans that modulate host immunity (as reviewed in (26)), it is critical to produce recombinant immunomodulatory molecules that harbour as similar glycosylation pattern as possible to the native ones. By exploiting the flexible N-glycosylation machinery of *Nicotiana benthamiana* plants, we successfully produced large amounts of recombinant ω1 carrying a terminal single branch Le^X-motif (pLe^X-ω1), a carbohydrate structure found on native ω1, making this glyco-engineered molecule more potent in Th2 skewing than the wild-type plant-glycosylated recombinant ω1 (pWT-ω1) (27). In the present study, we therefore investigate the effects and underlying mechanisms of these two plant-produced recombinant ω1 molecules on whole-body metabolic homeostasis in HFD-fed obese mice. Remarkably, treatment with both molecules improved the metabolic homeostasis of obese mice, an effect independent from the Th2 response but associated with a significant reduction in food intake. This raises the possibility that these glycoproteins can modulate the neuro-immunological axis involved in the control of feeding behaviour in mice.

MATERIALS AND METHODS

Animals, diet and treatment

All mouse experiments were performed in accordance with the Guide for the Care and Use of Laboratory Animals of the Institute for Laboratory Animal Research and have received approval from the university Ethical Review Boards (Leiden University Medical Center, Leiden, The Netherlands; DEC12199). 8-10 week-old male C57BL/6J mice (Charles River, L'Arbresle, France) were housed in a temperature-controlled room with a 12 hour light-dark cycle. Throughout the experiment, food and tap water were available *ad libitum*. Mice were fed a high-fat diet (HFD, 45% energy derived from fat, D12451, Research Diets) or a low-fat diet (LFD, 10% energy derived from fat, D12450B, Research Diets, Wijk bij Duurstede, The Netherlands) for 12 weeks, followed by group randomization according to body weight, fat mass, and fasting plasma glucose levels.

Recombinant omega-1 was produced in either wild-type (pWT-ω1) or Le^X-glyco-engineered *N. benthamiana* plants (pLe^X-ω1), as described previously (27). Recombinant pWT/pLe^X-ω1 (50 µg) and vehicle control (sterile-filtered 0.9% phosphate-buffered saline) were injected intraperitoneally every 3 days for 4 weeks, in four independent experiments. Short-term effects of pWT/pLe^X-ω1 were assessed in LFD- or HFD-fed mice treated every 2 days with 50 µg pWT/pLe^X-ω1 for one week. Dose-dependent effects of pLe^X-ω1 treatment were investigated by treating HFD-fed mice with 10, 25 or 50 µg of pLe^X-ω1 every 3 days for 4 weeks.

To investigate the role of type 2 immunity in the immunometabolic effects of pLe^X-ω1, 8-10 weeks-old male wild-type (WT) and *Stat6*$^{-/-}$ mice on C57BL/6J background (The Jackson Laboratory, Bar Harbor, ME, USA) were randomized based on body weight and fasting blood glucose levels, and either put on a HFD (60% energy derived from fat; D12492; Research Diets, New Brunswick, NJ, USA) or LFD (10% energy derived from fat; D12450J; Research Diets) for 10 weeks. To exclude effects of genotype-dependent microbiota differences on metabolic and immunological outcomes, the beddings of LFD- and HFD-fed WT and *Stat6*$^{-/-}$ mice were frequently mixed within similar diet groups throughout the run-in period. After 10 weeks, HFD-fed mice were randomized as described above and treated i.p. every 3 days for 4 weeks with 50 µg pLe^X-ω1 or vehicle-control.

Body composition and indirect calorimetry

Body composition was measured by MRI using an EchoMRI (Echo Medical Systems, Houston, TX, USA). Groups of 4-8 mice with free access to food and water were subjected to individual indirect calorimetric measurements during the initiation of the treatment with recombinant ω1 for a period of 7 consecutive days using a Comprehensive Laboratory Animal Monitoring System (Columbus Instruments, Columbus, OH, USA). Before the start of the measurements, single-housed animals were acclimated to the cages for a period of 48 h. Feeding behaviour was assessed by real-time food intake. Oxygen consumption and carbon dioxide production were measured at 15-min intervals. Energy expenditure (EE) was calculated and normalized for lean body mass (LBM), as previously described (18). Spontaneous locomotor activity was determined by the measurement of beam breaks.

At sacrifice, visceral white adipose tissue (epididymal; eWAT), subcutaneous white adipose tissue (inguinal; iWAT), supraclavicular brown adipose tissue (BAT) and liver were weighed and collected for further processing.

Plasma analysis

Blood samples were collected from the tail tip of 4h-fasted mice (food removed at 9 am) using chilled paraoxon-coated capillaries. Blood glucose level was determined using a Glucometer (Accu-Check; Roche Diagnostics, Almere, The Netherlands) and plasma insulin level was measured using a commercial kit according to the instructions of the manufacturer (Chrystal Chem, Zaandam, The Netherlands). The homeostatic model assessment of insulin resistance (HOMA-IR) adapted to mice was calculated as ((glucose (mg/dl)*0.055) × (insulin (ng/ml) × 172.1))/3857 and used as a surrogate measure of whole-body insulin resistance (28). The plasma concentrations of alanine aminotransferase (ALAT) was measured using a Reflotron® kit (Roche diagnostics) using a pool of plasma samples from each group (n = 4-6 mice per group) in 2 separate experiments.

Glucose and insulin tolerance tests

Whole-body insulin sensitivity was determined by an i.p. insulin tolerance test (ipITT) at week 1 or week 3 of treatment, as described previously (18). In short, after an initial blood

collection (t = 0), an i.p. bolus of insulin (1 U/kg (lean) body mass of insulin (NOVORAPID, Novo Nordisk, Alphen aan den Rijn, Netherlands)) was administered to 4h-fasted mice. Blood glucose was measured by tail bleeding at 20, 40, 60, and 90 min after insulin administration using a Glucometer.

Whole-body glucose tolerance was assessed by an i.p. glucose tolerance test at week 3 of treatment, as previously reported (18). After an initial blood collection (t = 0), a glucose load (2 g/kg total body weight of D-Glucose (Sigma-Aldrich, Zwijndrecht, The Netherlands)) was administered to 6h-fasted mice, and blood glucose was measured by tail bleeding at 20, 40, 60, and 90 min after glucose administration using a Glucometer. In addition, blood was collected at t = 20 minutes post glucose injection for assessing glucose-induced insulin secretion.

Isolation of stromal vascular fraction from adipose tissue

Epididymal adipose tissues were collected at sacrifice after a one minute perfusion with PBS through the heart left ventricle and digested as described previously (18). In short, collected tissues were digested for 1 h at 37°C in HEPES buffer (pH 7.4) containing 0.5 g/L collagenase type I from *Clostridium histolyticum* (Sigma-Aldrich) and 2% (w/v) dialyzed bovine serum albumin (BSA, fraction V; Sigma-Aldrich). The disaggregated adipose tissue was passed through a 100 µm cell strainer that was washed with PBS supplemented with 2.5 mM EDTA and 5% FCS. After centrifugation (350 x g, 10 minutes at room temperature), the supernatant was discarded and the pellet was treated with erythrocyte lysis buffer. The cells were next washed with PBS supplemented with 2.5 mM EDTA and 5% FCS, and counted manually.

Isolation of leukocytes from liver tissue

Livers were collected and digested as described previously (18). In short, livers were minced and digested for 45 minutes at 37°C in RPMI 1640 + Glutamax (Life Technologies, Bleiswijk, The Netherlands) containing 1 mg/mL collagenase type IV from *Clostridium histolyticum*, 2000 U/mL DNase (both Sigma-Aldrich) and 1 mM $CaCl_2$. The digested liver tissues were passed through a 100 µm cell strainer that was washed with PBS/EDTA/FCS. Following centrifugation (530 x g, 10 minutes at 4°C), the supernatant was discarded, after which the pellet was resuspended in PBS/EDTA/FCS and centrifuged at 50 x g to pellet hepatocytes (3 minutes at 4°C). Next, supernatants were collected and pelleted (530 x g, 10 minutes at 4°C). The cell pellet was first treated with erythrocyte lysis buffer and next washed with PBS/EDTA/FCS. $CD45^+$ leukocytes were isolated using LS columns and CD45 MicroBeads (35 µL beads per liver, Miltenyi Biotec) according to manufacturer's protocol and counted manually.

Processing of isolated immune cells for flow cytometry

For analysis of macrophage and lymphocyte subsets, both WAT stromal vascular cells and liver leukocytes were stained with the live/dead marker Aqua (Invitrogen), fixed with

either 1.9% paraformaldehyde (Sigma-Aldrich) or the eBioscience™ Intracellular fixation and permeabilization kit (Invitrogen), and stored in FACS buffer (PBS, 0.02% sodium azide, 0.5% FCS) at 4°C in the dark until subsequent analysis. For analysis of cytokine production, isolated cells were cultured for 4 hours in culture medium in the presence of 100 ng/mL phorbol myristate acetate, 1 µg/mL ionomycin and 10 µg/mL Brefeldin A (all from Sigma-Aldrich). After culture, cells were washed with PBS, stained with Aqua, and fixed as described above.

Flow cytometry

For analysis of CD4 T cells and innate lymphoid cell (ILC) subsets, SVF cells were stained with antibodies against B220 (RA3-6B2), CD11b (M1/70), CD3 (17A2), CD4 (GK1.5), NK1.1 (PK136) and Thy1.2 (53-2.1; eBioscience, San Diego, CA, USA), and CD11c (HL3) and GR-1 (RB6-8C5; both BD Biosciences, San Jose, CA, USA). For analysis of ILC2s, antibodies against CD25 (PC61.5; eBioscience), T1/ST2 conjugated to biotin (DJ8; MD Bioscience) and streptavidin-APC (BD Biosciences) as second staining were additionally included.

CD4 T cell subsets and cytokine production by ILCs were analyzed following permeabilization with either 0.5% saponin (Sigma-Aldrich) or eBioscience™ Intracellular fixation and permeabilization kit. Subsets were identified using antibodies against CD11b, CD11c, GR-1, B220, NK1.1, CD3, CD45, CD4, Thy1.2, IL-4 (11B11), IL-13 (eBio13A), Foxp3 (FJK-16s; all eBioscience), IL-5 (TRFK5) and IFN-γ (XMG1.2; both Biolegend).

For analysis of macrophages, eosinophils, monocytes and neutrophils, cells were permeabilized as described above. Cells were then incubated with an antibody against YM1 conjugated to biotin (polyclonal; R&D Systems, Minneapolis, MN, USA), washed, and stained with streptavidin-PerCP (BD Biosciences), and antibodies directed against CD45, CD11b, CD11c (HL3 (BD Biosciences) or N418 (Biolegend)), F4/80 (BM8; eBioscience or Biolegend), SiglecF (E50-2440; BD Biosciences), and Ly6C (HK1.4; Biolegend).

All cells were stained and measured within 4 days post fixation. Flow cytometry was performed using a FACSCanto or LSR-II (both BD Biosciences), and gates were set according to Fluorescence Minus One (FMO) controls. Representative gating schemes are shown in Figure S1.

RNA purification and qRT-PCR

RNA was extracted from snap-frozen adipose tissue samples (~20 mg) using Tripure RNA Isolation reagent (Roche Diagnostics, Almere, The Netherlands). Total RNA (1 µg) was reverse transcribed and quantitative real-time PCR was then performed with SYBR Green Core Kit on a MyIQ thermal cycler (Bio-Rad) using specific primers sets (available on request). mRNA expression was normalized to ribosomal protein, large, P0 (RplP0) mRNA content and expressed as fold change compared to LFD-fed mice using the ΔΔCT method.

Hepatic triglyceride content

Liver lipids were extracted as previously described (29). Briefly, small liver samples were homogenized in ice-cold methanol. After centrifugation, lipids were extracted by addition of 1800 µl CH3OH:CHCl3 (1:3 v/v) to 45 µl homogenate, followed by vigorous vortexing and phase separation by centrifugation (14,000 rpm; 15 min at RT). The organic phase was dried and dissolved in 2% Triton X-100 in water. Triglycerides concentrations were measured using a commercially available enzymatic kit (Instruchemie, Delfzijl, the Netherlands) and expressed as nanomoles per mg protein, which was determined using the Bradford protein assay kit (Sigma-Aldrich).

Histological analysis

A piece of liver was fixed in 4% paraformaldehyde (PFA; Sigma-Aldrich), paraffin-embedded, sectioned at 4 µm and stained with Hematoxilin and Eosin (H&E), or Sirius Red to visualize collagen. Six fields at 20x magnification (total area 1.68 mm^2) were used for the analysis of hepatic steatosis in H&E-stained sections. On Sirius Red-stained sections, fibrosis was scored on 10 fields at 40x magnification (total area 1.23 mm^2) as absent (score 0), present in the perisinusoidal or periportal area (score 1), present in the perisinusoidal and periportal (score 2), bridging fibrosis (score 3) or cirrhosis (score 4) as described elsewhere (30).

Statistical analysis

All data are presented as mean ± standard error of the mean (SEM). Statistical analysis was performed using GraphPad Prism version 7.04 for Windows (GraphPad Software, La Jolla, CA, USA) with ordinary one-way analysis of variance (ANOVA) followed by Bonferroni post-hoc test. Differences between groups were considered statistically significant at $P < 0.05$.

RESULTS

Plant-produced recombinant omega-1 glycovariants reduce body weight and improve whole-body metabolic homeostasis in obese mice

To study the effects of recombinant ω1 glycovariants on whole-body metabolic homeostasis, C57BL/6J mice were fed a LFD or HFD for 12 weeks and next treated biweekly with intraperitoneal injections of 50 µg pWT-ω1, pLe^X-ω1 or PBS (vehicle-control) for 4 weeks. Both ω1 glycovariants induced a rapid and gradual body weight loss in HFD-fed mice (Fig. 1A-B), which was exclusively due to a decrease in fat mass (Fig. 1C) whereas lean mass was not affected (Fig. 1D). pWT/pLe^X-ω1 significantly reduced epididymal white adipose tissue (eWAT) mass but had no effect on liver, subcutaneous white adipose tissue (iWAT) and brown adipose tissue (BAT) masses (Fig. 1E). Using metabolic cages, we found that both ω1 glycovariants induced a significant decrease in cumulative food intake during

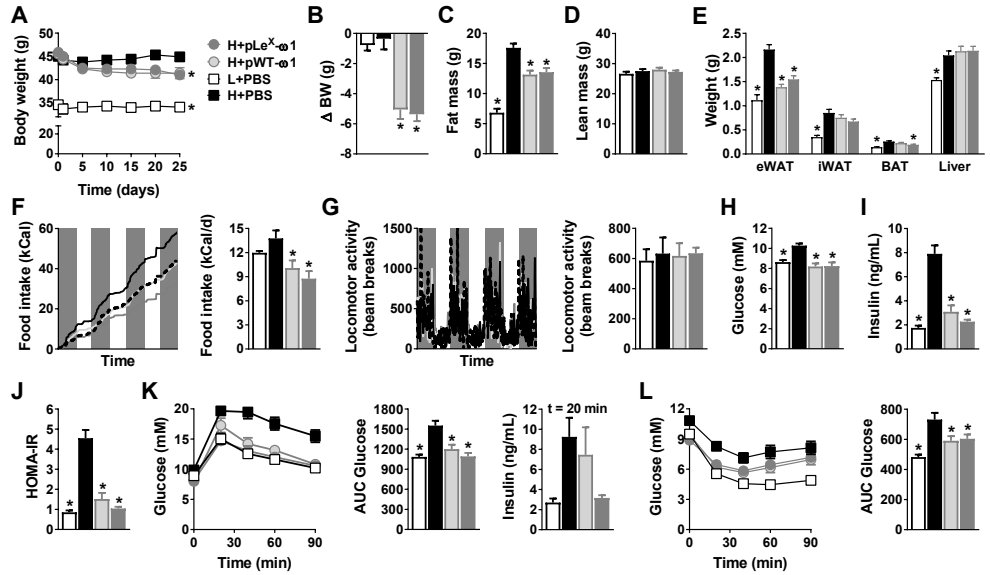

Figure 1. Plant-produced recombinant ω1 glycovariants reduce body weight, visceral fat mass and food intake in diet-induced obese mice. Mice were fed a LFD or a HFD for 12 weeks, after which they were treated i.p. with PBS, or 50 µg pWT-ω1 or pLe^X-ω1 once every 3 days for a period of 4 weeks. Body weight was monitored throughout the experimental period (*A-B*). Body composition (*C-D*) and weight of epididymal WAT (eWAT), inguinal WAT (iWAT), instrascapular brown adipose tissue (BAT) and the liver (*E*) were measured after 4 weeks of treatment. Food intake was assessed using fully automated single-housed metabolic cages during the first week of treatment (*F*). Locomotor activity was determined by measuring by beam breaks (*G*). Blood glucose (*H*) and plasma insulin levels (*I*) were determined in 4h-fasted mice during week 4 of treatment and HOMA-IR was calculated (*J*). An i.p. glucose tolerance test (2 g/kg body weight) was performed in 6h-fasted mice at week 3 of treatment. Blood glucose levels were measured at the indicated time points and the AUC of the glucose excursion curve was calculated (*K*). Blood was also collected for determination of glucose-induced insulin secretion at t = 20 minutes post glucose injection (*K*). An i.p. insulin tolerance test (1U/kg lean body mass) was performed in 4h-fasted mice at week 3 of treatment. Blood glucose levels were measured at the indicated time points and the area under the curve (AUC) of the glucose excursion curve was calculated (*L*). Data shown are a pool of 2 (D) or 4 (A-E, H-L) independent experiments. Results are expressed as means ± SEM. * *P*<0.05 *vs* HFD (n = 12-20 animals per group in A-E, K-L, and 4-13 animals per group in F-J).

the experimental period (Fig. 1F). Consequently, mean daily energy intake was reduced to the same extent while locomotor activity was not affected (Fig. 1G).

We next investigated the effects of pWT/pLe^X-ω1 on whole-body metabolic homeostasis. As expected, HFD-feeding increased fasting blood glucose, plasma insulin and homeostatic model assessment of insulin resistance (HOMA-IR) as compared to LFD-fed mice (Fig. 1H-J). Remarkably, treatment with both ω1 glycovariants for 4 weeks significantly reduced blood glucose and insulin in obese mice to the levels of LFD-fed lean mice (Fig. 1H-I). As a result, HOMA-IR was significantly reduced in ω1-treated mice, indicating a better insulin sensitivity with a trend towards a stronger effect induced by

the recombinant molecule harbouring single branch Le^X (Fig. 1J). Congruent with these data, we observed a significant improvement in whole-body glucose tolerance (Fig. 1K) and insulin sensitivity (Fig. 1L) in both pWT and pLe^X-ω1-treated obese mice. Of note, the effects of these two ω1 glycovariants on plasma metabolic parameters and whole-body insulin sensitivity were already observed after one week of treatment, although there was only marginal impact on body weight and fat mass at this time point (Fig. S2). Furthermore, the improvement of metabolic homeostasis was found to be dose-dependent, at least for pLe^X-ω1 (Fig. S3). Altogether, these data show that both recombinant ω1 glycovariants improve whole-body metabolic homeostasis in insulin-resistant obese mice.

Omega-1 glycovariants increase adipose tissue Th2 cells, eosinophils and alternatively-activated macrophages, but not ILC2s

An ILC2-eosinophil-AAM axis contributes to the maintenance of adipose tissue insulin sensitivity in homeostatic conditions and is disrupted during obesity (14, 15). To investigate whether the beneficial metabolic effects induced by ω1 glycovariants could be due to an increase in these type 2 immune cells, we isolated the stromal vascular fraction (SVF) from eWAT and analysed the immune cell composition by flow cytometry (Fig. S1). We found that both ω1 glycovariants markedly increased WAT CD4 T cells, with pWT-ω1 being more potent than pLe^X-ω1, while total ILCs were unaffected (Fig. 2A). Interestingly, *ex vivo* restimulation revealed a specific increase in IL-4/5/13-expressing Th2 cells, while the other CD4 T cell subsets, *i.e.* regulatory T cells (Treg) and Th1 cells, were not affected (Fig. 2B). In addition, we confirmed that HFD reduced WAT IL-5$^+$/IL-13$^+$ ILC2s, as previously reported (14), an effect that was even further pronounced with ω1 glycovariants (Fig. 2C).

The type 2 cytokines IL-5 and IL-13 produced by either ILC2s and/or Th2 cells have been reported to maintain WAT eosinophils (14). Congruent with our data on Th2 cells, we found a potent increase in WAT eosinophils upon ω1 treatment that was of similar extent for both glycovariants (Fig. 2D). Finally, both pWT-ω1 and pLe^X-ω1 increased WAT Ym1$^+$ AAMs while the pro-inflammatory CD11c$^+$ macrophages were not affected, shifting the balance of cell polarization towards a M2/M(IL-4)-like phenotype (Fig. 2E-H). A similar immune response was already observed after one week of treatment with ω1 glycovariants (Fig. S4) and appears to be dose-dependent (Fig. S5).

Omega-1 glycovariants do not induce WAT beiging

Although the concept was recently challenged (31), AAMs have been suggested to trigger WAT beiging through production of catecholamines, thereby increasing energy expenditure (32-34). Since WAT AAMs were significantly increased in ω1-treated obese mice, we investigated whether the ω1 glycovariants could induce WAT beiging and therefore enhance adaptive thermogenesis and energy expenditure. We found that the recombinant molecules neither increased *Ucp1* or other beiging gene markers mRNA expression in both epididymal and subcutaneous (inguinal) fat pads (Fig. 3A-B), nor

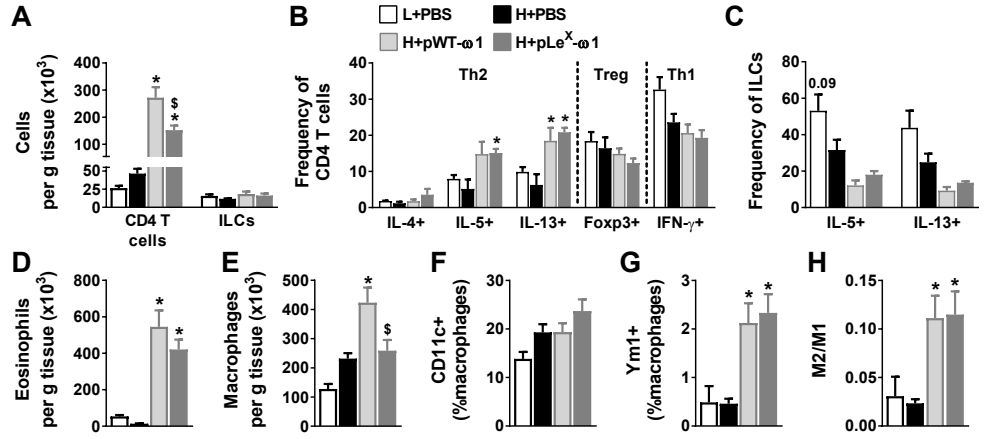

Figure 2. **ω1 glycovariants increase WAT Th2 cells, eosinophils and AAM, without affecting ILCs.** Mice were fed a LFD or a HFD and were treated with PBS or pWT/pLe^X-ω1 as described in the legend of Figure 1. At sacrifice (week 4 of treatment), eWAT was collected and the stromal vascular fraction (SVF) was isolated. Following fixation and permeabilization, SVF cells were stained and analyzed by flow cytometry. The complete gating strategy is shown in Figure S1. Numbers per gram tissue CD4 T cells, ILCs (*A*), eosinophils (*D*) and macrophages (*E*) were determined. Intracellular cytokine production was analyzed after 4h stimulation with PMA and ionomycin in the presence of Brefeldin A. CD4 T cells were identified as Aqua$^-$CD45$^+$Thy1.2$^+$Lineage$^+$CD4$^+$ cells, and ILCs were identified as Aqua$^-$CD45$^+$Thy1.2$^+$Lineage$^-$CD3$^-$CD4$^-$ cells, in which the lineage cocktail included antibodies against CD11b, CD11c, B220, GR-1, NK1.1 and CD3. Frequencies of CD4 T helper subsets (*B*) and cytokine-expressing ILCs (*C*) were determined. Percentages of CD11c$^+$Ym1$^-$ (M1-like; *F*) and CD11c$^-$Ym1$^+$ (M2-like; *G*) in macrophages. Using the percentages of M1-like and M2-like macrophages, M2/M1 ratios were calculated (*H*). Data shown are a pool of at least three independent experiments, except for C and E, which are a representative experiment of at least two independent experiments. Results are expressed as means ± SEM. * P<0.05 *vs* HFD, $ P<0.05 *vs* pWT-ω1 (n = 6-19 animals per group in A-B, D, F-I, and 3-9 animals per group in C and E).

the whole-body energy expenditure measured in metabolic cages (Fig. 3C), indicating that ω1 does not induce canonical or non-canonical WAT beiging in our conditions.

STAT6-mediated type 2 immunity is not required for the effects of pLe^X-ω1 on metabolic homeostasis

Induction of AAM polarization is a classical feature of type 2 immunity which usually occurs through IL-4/IL-13 receptor-mediated signalling and requires the transcription factor STAT6 (35, 36). In order to assess whether type 2 immunity is required for the metabolic effects of ω1, we therefore used Stat6-deficient mice. As expected, while pLe^X-ω1 increased WAT Th2 cells and AAMs in WT mice, this specific type 2 immune response was abrogated in Stat6$^{-/-}$ mice (Fig. 4A-B). However, treatment with pLe^X-ω1 still reduced body weight (Fig. 4C) and food intake (Fig. 4D) in Stat6$^{-/-}$ obese mice to the same extent as in WT mice. In addition, while pLe^X-ω1 did not significantly affect fasting blood glucose levels, both insulin levels and HOMA-IR were markedly decreased in both genotypes (Fig. 4E-G).

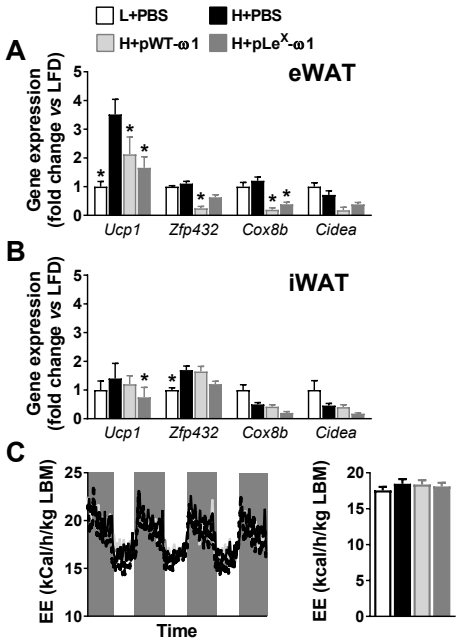

Figure 3. **ω1 glycovariants do not induce WAT beiging.** Mice were fed a LFD or a HFD and were treated with PBS or pWT/pLe^{X}-ω1 as described in the legend of Figure 1. At sacrifice, mRNA expression in eWAT (*A*) and iWAT (*B*) of the indicated genes was quantified by RT-PCR and expressed relative to the *RplP0* gene as fold difference compared to the LFD-fed mice. Energy expenditure, corrected for lean body mass, was measured using fully automated single-housed metabolic cages during the first week of treatment (*C*). Data shown are a pool of two independent experiments. Results are expressed as means ± SEM. * $P<0.05$ *vs* HFD (n = 4-10 animals per group).

Moreover, the improvements in whole-body glucose tolerance (Fig. 4H-I) and insulin sensitivity (Fig. 4J) was still observed in Stat6$^{-/-}$ mice, indicating that pLe^{X}-ω1 restored metabolic homeostasis in obese mice independent of its Th2-inducing capacity.

Omega-1 glycovariants do not affect hepatic steatosis, but increase fibrotic gene markers and liver damage

Similar to WAT, maintenance of hepatic insulin sensitivity is also associated with type 2 immunity (37). On the other hand, obesity-driven activation of Kupffer cells increases the recruitment of pro-inflammatory monocytes and triggers hepatic insulin resistance (2, 11). In our conditions, while pWT/pLe^{X}-ω1 increased Th2 cells in the liver, we surprisingly did not find alternative activation of Kupffer cells (Fig. 5A-D). Instead, the ω1 glycovariants increased the number of CD11c^{+} pro-inflammatory Kupffer cells (Fig. 5E-F) and newly recruited monocytes (Fig. 5G). However, ω1 glycovariants did not affect hepatic steatosis, as assessed by histomorphologic assessment of hematoxylin and eosin (H&E)-stained liver sections (Fig. 5H-I) and tissue triglycerides content (Fig. 5J).

In addition to ectopic lipid deposition in the liver during NAFLD, increased inflammation, hepatocyte damage and fibrosis may characterize progression towards non-alcoholic steatohepatitis (NASH) (38). IL-13 has recently also been implicated to play a role in the development of liver fibrosis (39, 40), hence we investigated whether ω1 glycovariants affect liver fibrosis. pLe^{X}-ω1 significantly increased fibrotic gene marker expression (Fig. 5K), while no clinical fibrosis was detected (Fig. 5L). However, we observed an increase in circulating alanine transaminase levels (Fig. 5M), which indicates enhanced liver damage.

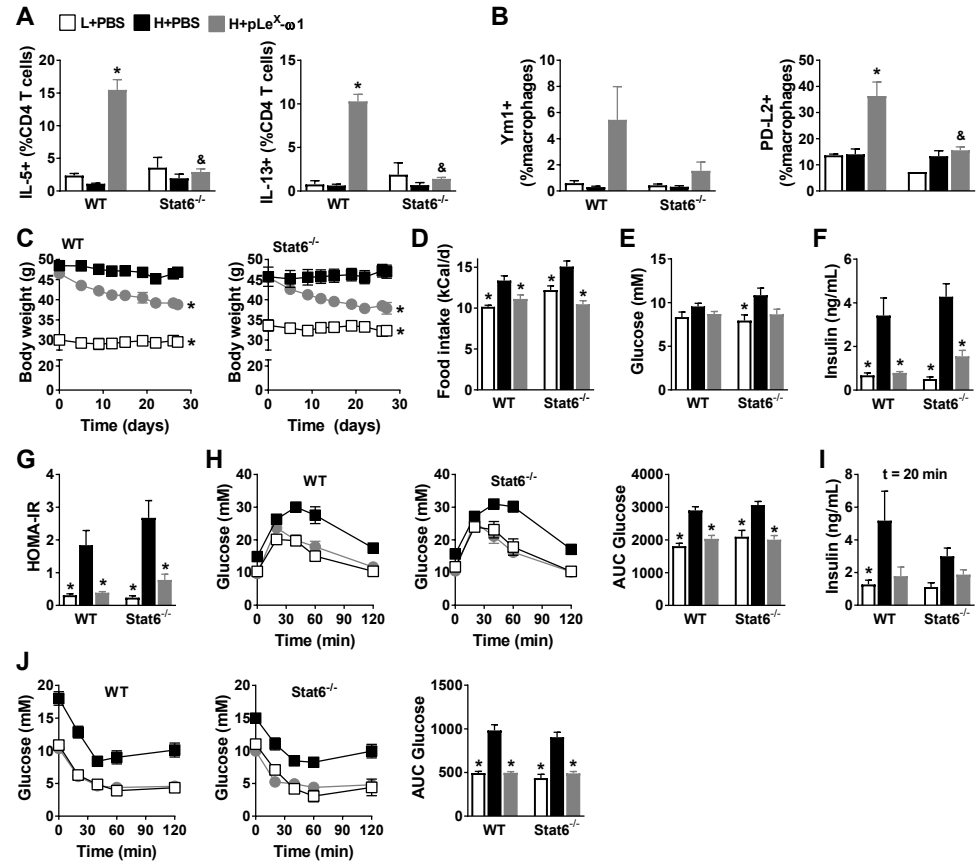

Figure 4. **STAT6 is not required for metabolic effects of pLe^{X}-ω1.** WT and Stat6-/- mice on a C57BL/6J background were fed a LFD or a HFD for 12 weeks before 4 weeks of biweekly intraperitoneal injections with PBS or 50 µg pLe^{X}-ω1. At the end of the experiment (week 4 of treatment), eWAT was collected, processed and analyzed as described in the legend of Figure 2. The frequencies of cytokine-expressing CD4 T cells were determined (*A*). Abundances of Ym1^{+} or PD-L2^{+} (M2-like) macrophages (*B*) were determined. Body weight (*C*) and food intake (*D*) was monitored throughout the experimental period. Blood glucose (*E*) and plasma insulin levels (*F*) were determined and HOMA-IR (*G*) was calculated as described in the legend of Figure 1. An i.p. glucose tolerance test (2 g/kg body weight; *H-I*) and i.p. insulin tolerance test (1U/kg body weight; *J*) were performed as described in the legend of Figure 1. Results are expressed as means ± SEM. *$P<0.05$ *vs* HFD, & $P<0.05$ *vs* WT (n = 3-5 animals per group for all measurements).

To investigate the role of type 2 immunity in the pro-fibrotic effects of pLe^{X}-ω1, we used Stat6-deficient mice. As expected, the increase in liver IL-13^{+} Th2 cells in response to pLe^{X}-ω1 was markedly reduced in Stat6-deficient mice (Fig. 5N). In line with this data, the increase in hepatic IL-13 gene expression induced by pLe^{X}-ω1 was also significantly reduced in obese Stat6$^{-/-}$ mice as compared to WT (Fig. 5O). Although pLe^{X}-ω1 still induced expression of fibrotic gene markers in Stat6-deficient mice, there was a marked decrease in expression as compared to WT mice (Fig. 5O), suggesting that recombinant

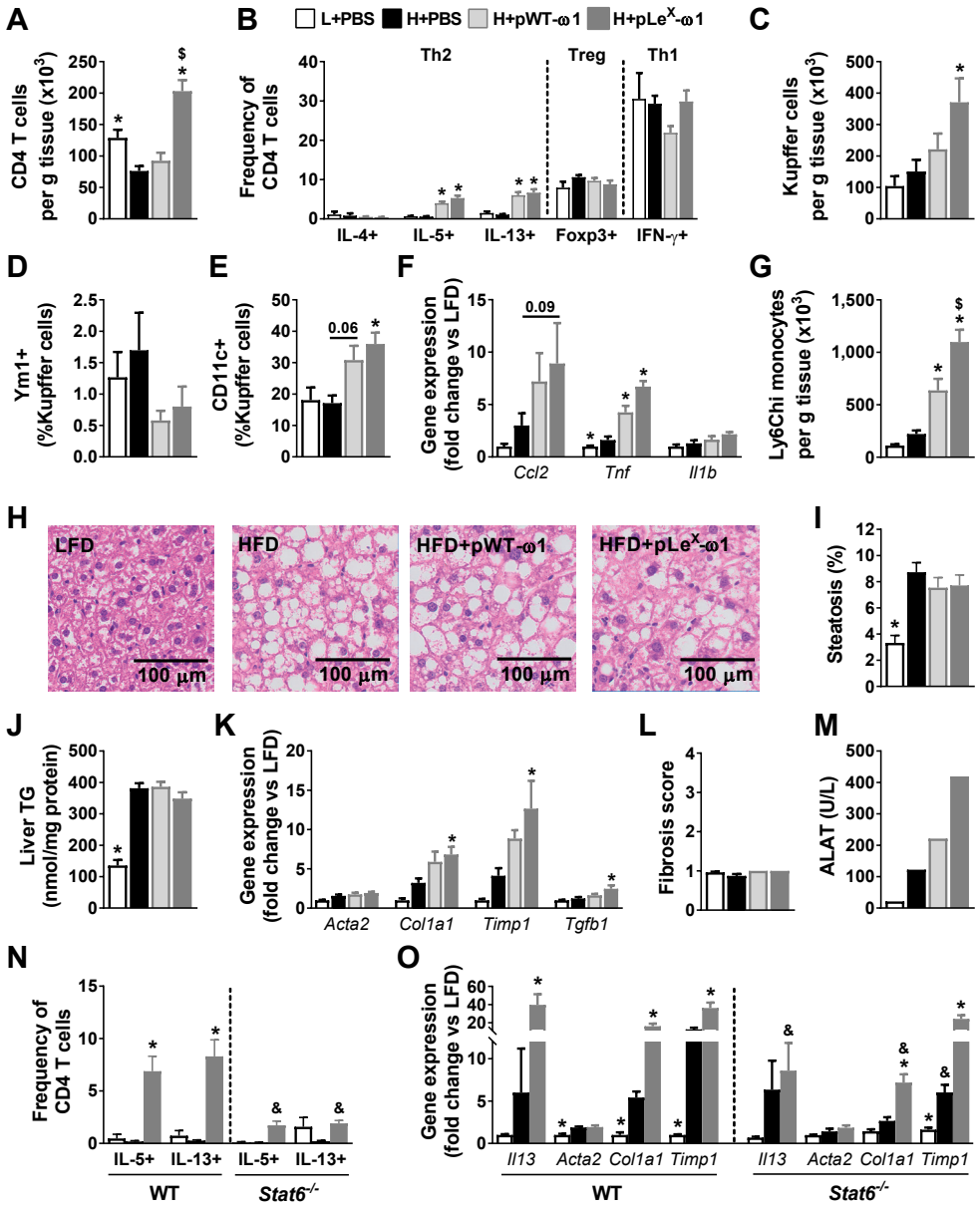

Figure 5. ω1 glycovariants do not affect hepatic steatosis, but increase fibrotic gene markers and liver damage. Mice were fed a LFD or a HFD and were treated with PBS or pWT/pLe^{X}-ω1 as described in the legend of Figure 1. At sacrifice, a small piece of liver was immediately snap-frozen for qPCR and liver lipid content analyses, and another piece was used for H&E staining. From the remaining liver, CD45^{+} liver cells were isolated and analyzed by flow cytometry. The cell numbers per gram tissue and abundances of CD4 T cells (*A*) and T helper subsets (*B*), Kupffer cells (*C*), macrophage phenotypes (*D-E*) and Ly6C^{hi} monocytes (*G*) were determined. mRNA expression of the indicated genes was analysed as described in the legend of figure 3 (*F*). H&E slides of the liver (*H*) were used for determining hepatic steatosis (*I*). Liver triglycerides were determined (*J*). mRNA expression of the indicated genes was analysed as described in the legend of Figure 3 (*K*). Sirius Red-stained sections were scored for fibrosis (*L*). Plasma alanine aminotransferase levels (*M*) were determined. WT and Stat6-/- mice were fed a LFD or a HFD and were treated as described in the legend of Figure 4. Frequencies of IL-5/IL-13-expressing CD4 T cells were determined (*N*). mRNA expression of the indicated genes was analysed as described in the legend of figure 3 (*O*). Data shown are a pool of at least two independent experiments, except for N-O. Results are expressed as means ± SEM. * $P<0.05$ *vs* HFD, $ $P<0.05$ *vs* pWT-ω1 (n 5=18 animals per group in A-M, and 3-5 animals per group in N-O).

ω1 induces fibrotic gene markers at least partly through type 2 immunity. Taken together, these results show that recombinant ω1 glycovariants improve whole-body metabolic homeostasis independent of their Th2 inducing capacity, while simultaneously inducing early markers of mild hepatic fibrosis.

DISCUSSION

Type 2 immunity is involved in the maintenance of metabolic homeostasis and its disruption during obesity promotes chronic low-grade inflammation, associated with insulin resistance (1). Since helminths induce type 2 immunity, the association between helminths and their potential effects on insulin sensitivity and glucose homeostasis has gained increasing attention (41), accompanied by the search for single helminth-derived molecules that are capable of driving the type 2 immune response (20). The glycoprotein omega-1, a T2 ribonuclease which is secreted from *S. mansoni* eggs, has previously been identified as the major immunomodulatory component in SEA (23, 24) and was shown to condition dendritic cells to prime Th2 responses, as least partly through its glycan-mediated uptake and intracellular RNase activity (24). Here, we report that two plant-produced recombinant ω1 glycovariants induced a rapid and sustained reduction in body weight and improved HOMA-IR, whole-body insulin sensitivity and glucose tolerance in obese mice. Although both ω1 glycovariants induced a strong type 2 immune response in WAT, characterized by a significant increase in Th2 cells, eosinophils and AAMs, the beneficial effect on metabolic homeostasis was still present in Stat6-deficient obese mice, indicating that improvements of insulin sensitivity and glucose tolerance occurred independently of the Th2-inducing capacity of ω1. These findings indicate that helminth derived molecules may act through multiple distinct pathways that can improve metabolic homeostasis. Interestingly, a trend for a stronger effect on insulin sensitivity was observed with pLe^{X}–ω1, whose glycans resemble the ones of native helminth ω1 the most, whereas the improvement of glucose tolerance was similar to pWT–ω1.

A recent study from Hams et al. reported that acute treatment of HFD-fed obese mice with HEK-293-produced recombinant ω1 induced long-lasting weight loss, and improved glucose tolerance by a mechanism involving IL-33-mediated increase in WAT ILC2s and adipose beiging (25). However, in contrast to this finding, we only observed a slight increase in IL-33 expression in eWAT (data not shown) and no increase in WAT

ILC2s after either one, or four weeks of treatment with plant-produced ω1 glycovariants. Moreover, we did not find any evidence of WAT beiging in both eWAT and iWAT from obese mice treated with ω1 glycovariants. Importantly, it should be noted that despite similar RNase activities when compared to native ω1 (27), the recombinant ω1 produced by HEK-293 cells and the glyco-engineered ones from tobacco plants harbor significantly different N-glycosylation patterns (23, 24). Finally, on top of differences in treatment regimen (2 injections in 4 days *versus* bi-weekly injection for 4 weeks in our study), it is worth mentioning that in Hams et al. the effects of HEK-produced ω1 were compared to the effects of ovalbumin (25), which is an immunomodulatory molecule by itself, differing significantly from our experimental condition where a neutral vehicle (PBS) was used as control.

Both ω1 glycovariants were found to induce a type 2 immune response in WAT, characterized by a significant increase in Th2 cells, eosinophils and AAMs. In our study, as previously described for SEA (18), the ω1-induced increase in type 2 cytokines was shown to be clearly derived from $CD4^+$ T cells, not ILC2s. Our data indicate that both pWT–ω1 and pLe^X–ω1 require Th2 cells, rather than ILC2s to induce WAT eosinophilia and AAM polarization. It was previously shown that pLe^X–ω1, compared to pWT-ω1, induced a stronger Th2 polarization *in vivo* using a footpad immunization model in mice (27). In our conditions, both glycovariants induced a similar increase in the percentage of Th2 cells in metabolic tissue from obese mice, whereas pLe^X–ω1 increased total $CD4^+$ T cells to a greater extent in the liver and to a lesser extent in WAT when compared to pWT-ω1. Altogether, this suggests that the glycosylation pattern of ω1 might induce tissue-specific differences in total Th2 cells.

In the liver, ω1 glycovariants increased IL-13-producing Th2 cells but, unlike SEA (18), promoted CD11c expression in Kupffer cells while not affecting the expression of Ym1, suggesting that macrophages are rather polarized towards a pro-inflammatory state. Of note, ω1 glycovariants also increased hepatic expression of fibrotic gene markers and circulating ALAT levels, both indicating increased liver damage. Interestingly, the pLe^X–ω1-induced increase in liver IL-13^+ Th2 cells and hepatic IL-13 gene expression were markedly reduced in Stat6-deficient mice, which was accompanied by a decreased expression of fibrotic gene markers. Collectively, these findings confirmed previous studies in which IL-13 was shown to play a role in the development of liver fibrosis (39, 40).

As the type 2 immune response seems not to be significantly involved in the beneficial metabolic effects of ω1, the question of the underlying mechanism(s) remains. Interestingly, we found that treatment with both ω1 glycovariants significantly reduced food intake, with a trend for pLe^X–ω1 being more potent than pWT–ω1. Furthermore, this anorexigenic effect of ω1, which was not observed previously when mice were chronically infected with *S. mansoni* or treated with SEA (18), was dose-dependent (already detectable at a concentration of 10 µg) and also present in Stat6-deficient mice. Altogether, these findings lead us to the hypothesis that the beneficial metabolic effects of ω1 might be mediated through a reduction in food intake, rather than an increase in type 2 immune

cells. Of note, in the study from Hams et al. using HEK-produced ω1, the authors claimed that treatment with this recombinant molecule in obese mice did not significantly affect food intake, but unfortunately these crucial data were not shown (25).

Since both locomotor activity and lean body mass were not affected by ω1, we also conclude that the reduced food intake was not related to wasting or illness (as reviewed in (42)). In order to assess the contribution of reduced food intake to the metabolic benefits of recombinant ω1, paired-feeding could be used in future studies. In addition, in search for underlying mechanisms, it will be important to study the biodistribution of ω1 using labeled molecules, notably to investigate whether the molecules can be detected in brain areas known to be involved in the control of food intake, such as the hypothalamus (43). In line with this, it would be interesting to assess the effect of ω1 on the hypothalamic expression of anorexigenic (e.g. POMC, CART) and orexigenic (e.g. NPY, AgRP) peptides.

In conclusion, our work has revealed that the improvement of metabolic homeostasis in insulin-resistant obese mice by plant-produced recombinant ω1 glycovariants is independent of their Th2-inducing capacities.

Our current hypotheses are that the beneficial metabolic effects of ω1 could be explained by brain-mediated food intake and/or immune-independent direct interaction of ω1 with metabolic cells. Further studies are undoubtedly required to unravel these underlying mechanisms. Of note, with regards to the therapeutic potential of ω1 as treatment for metabolic disorders, it is important to cautiously underline that recombinant ω1 induced early markers of mild hepatic fibrosis, by a mechanism partly mediated through ω1-induced type 2 immunity.

REFERENCES

1. Donath MY, Shoelson SE. Type 2 diabetes as an inflammatory disease. Nat Rev Immunol 2011; 11(2): 98-107.
2. Lackey DE, Olefsky JM. Regulation of metabolism by the innate immune system. Nat Rev Endocrinol 2016; 12(1): 15-28.
3. Heilbronn LK, Campbell LV. Adipose tissue macrophages, low grade inflammation and insulin resistance in human obesity. Curr Pharm Des 2008; 14(12): 1225-30.
4. Kolb H, Mandrup-Poulsen T. The global diabetes epidemic as a consequence of lifestyle-induced low-grade inflammation. Diabetologia 2010; 53(1): 10-20.
5. Lumeng CN, DelProposto JB, Westcott DJ, Saltiel AR. Phenotypic switching of adipose tissue macrophages with obesity is generated by spatiotemporal differences in macrophage subtypes. Diabetes 2008; 57(12): 3239-46.
6. Obstfeld AE, Sugaru E, Thearle M, et al. C-C chemokine receptor 2 (CCR2) regulates the hepatic recruitment of myeloid cells that promote obesity-induced hepatic steatosis. Diabetes 2010; 59(4): 916-25.
7. Morinaga H, Mayoral R, Heinrichsdorff J, et al. Characterization of distinct subpopulations of hepatic macrophages in HFD/obese mice. Diabetes 2015; 64(4): 1120-30.
8. Fink LN, Oberbach A, Costford SR, et al. Expression of anti-inflammatory macrophage genes within skeletal muscle correlates with insulin sensitivity in human obesity and type 2 diabetes. Diabetologia 2013; 56(7): 1623-8.
9. Fink LN, Costford SR, Lee YS, et al. Pro-inflammatory macrophages increase in skeletal muscle of high fat-fed mice and correlate with metabolic risk markers in humans. Obesity (Silver Spring) 2014; 22(3): 747-57.
10. Kratz M, Coats BR, Hisert KB, et al. Metabolic dysfunction drives a mechanistically distinct proinflammatory phenotype in adipose tissue macrophages. Cell Metab 2014; 20(4): 614-25.
11. Lanthier N, Molendi-Coste O, Horsmans Y, van Rooijen N, Cani PD, Leclercq IA. Kupffer cell activation is a causal factor for hepatic insulin resistance. Am J Physiol Gastrointest Liver Physiol 2010; 298(1): G107-16.
12. Talukdar S, Oh DY, Bandyopadhyay G, et al. Neutrophils mediate insulin resistance in mice fed a high-fat diet through secreted elastase. Nat Med 2012; 18(9): 1407-12.
13. Cai D, Yuan M, Frantz DF, et al. Local and systemic insulin resistance resulting from hepatic activation of IKK-beta and NF-kappaB. Nat Med 2005; 11(2): 183-90.
14. Molofsky AB, Nussbaum JC, Liang HE, et al. Innate lymphoid type 2 cells sustain visceral adipose tissue eosinophils and alternatively activated macrophages. J Exp Med 2013; 210(3): 535-49.
15. Wu D, Molofsky AB, Liang HE, et al. Eosinophils sustain adipose alternatively activated macrophages associated with glucose homeostasis. Science 2011; 332(6026): 243-7.
16. Maizels RM, Yazdanbakhsh M. Immune regulation by helminth parasites: cellular and molecular mechanisms. Nature reviews Immunology 2003; 3(9): 733-44.
17. Wiria AE, Hamid F, Wammes LJ, et al. Infection with Soil-Transmitted Helminths Is Associated with Increased Insulin Sensitivity. PLoS One 2015; 10(6): e0127746.
18. Hussaarts L, Garcia-Tardon N, van Beek L, et al. Chronic helminth infection and helminth-derived egg antigens promote adipose tissue M2 macrophages and improve insulin sensitivity in obese mice. FASEB journal : official publication of the Federation of American Societies for Experimental Biology 2015; 29(7): 3027-39.
19. Okano M, Satoskar AR, Nishizaki K, Abe M, Harn DA, Jr. Induction of Th2 responses and IgE is largely due to carbohydrates functioning as adjuvants on Schistosoma mansoni egg antigens. J Immunol 1999; 163(12): 6712-7.
20. Hussaarts L, Yazdanbakhsh M, Guigas B. Priming dendritic cells for th2 polarization: lessons learned from helminths and implications for metabolic disorders. Front Immunol 2014; 5: 499.
21. Ritter M, Gross O, Kays S, et al. Schistosoma mansoni triggers Dectin-2, which activates the Nlrp3 inflammasome and alters adaptive immune responses. Proc Natl Acad Sci U S A 2010; 107(47): 20459-64.
22. Kaisar MMM, Ritter M, Del Fresno C, et al. Dectin-1/2-induced autocrine PGE2 signaling licenses dendritic cells to prime Th2 responses. PLoS Biol 2018; 16(4): e2005504.
23. Everts B, Perona-Wright G, Smits HH, et al. Omega-1, a glycoprotein secreted by Schistosoma mansoni eggs, drives Th2 responses. J Exp Med 2009; 206(8): 1673-80.
24. Everts B, Hussaarts L, Driessen NN, et al. Schistosome-derived omega-1 drives Th2 polarization by suppressing protein synthesis following internalization by the mannose receptor. J Exp Med 2012; 209(10): 1753-67, S1.
25. Hams E, Bermingham R, Wurlod FA, et al. The helminth T2 RNase omega1 promotes metabolic homeostasis in an IL-33- and group 2 innate lymphoid cell-dependent mechanism. FASEB journal : official publication of the Federation of American Societies for Experimental Biology 2016; 30(2): 824-35.
26. Hokke CH, Yazdanbakhsh M. Schistosome glycans and innate immunity. Parasite Immunol 2005; 27(7-8): 257-64.
27. Wilbers RH, Westerhof LB, van Noort K, et al. Production and glyco-engineering of immunomodulatory helminth glycoproteins in plants. Sci Rep 2017; 7: 45910.
28. Lee S, Muniyappa R, Yan X, et al. Comparison between surrogate indexes of insulin sensitivity and resistance and hyperinsulinemic euglycemic clamp estimates in mice. Am J Physiol Endocrinol Metab 2008; 294(2): E261-70.
29. Geerling JJ, Boon MR, van der Zon GC, et al. Metformin lowers plasma triglycerides by promoting VLDL-triglyceride clearance by brown adipose tissue in mice. Diabetes 2014; 63(3): 880-91.
30. Kleiner DE, Brunt EM, Van Natta M, et al. Design and validation of a histological scoring system for nonalcoholic fatty liver disease. Hepatology 2005; 41(6): 1313-21.
31. Fischer K, Ruiz HH, Jhun K, et al. Alternatively activated macrophages do not synthesize catecholamines or contribute to adipose tissue adaptive thermogenesis. Nat Med 2017; 23(5): 623-30.
32. Nguyen KD, Qiu Y, Cui X, et al. Alternatively activated macrophages produce catecholamines to sustain adaptive thermogenesis. Nature 2011; 480(7375): 104-8.
33. Qiu Y, Nguyen KD, Odegaard JI, et al. Eosinophils and type 2 cytokine signaling in macrophages orchestrate development of functional beige fat. Cell 2014; 157(6): 1292-308.
34. Lee MW, Odegaard JI, Mukundan L, et al. Activated type 2 innate lymphoid cells regulate beige fat biogenesis. Cell 2015; 160(1-2): 74-87.
35. Loke P, Allison JP. PD-L1 and PD-L2 are differentially regulated by Th1 and Th2 cells. Proc Natl Acad Sci U S A 2003; 100(9): 5336-41.
36. Huber S, Hoffmann R, Muskens F, Voehringer D. Alternatively activated macrophages inhibit T-cell proliferation by Stat6-dependent expression of PD-L2. Blood 2010; 116(17): 3311-20.
37. Ricardo-Gonzalez RR, Red Eagle A, Odegaard JI, et al. IL-4/STAT6 immune axis regulates peripheral nutrient metabolism and insulin sensitivity. Proc Natl Acad Sci U S A 2010; 107(52): 22617-22.
38. Koyama Y, Brenner DA. Liver inflammation and fibrosis. J Clin Invest 2017; 127(1): 55-64.
39. Gieseck RL, 3rd, Ramalingam TR, Hart KM, et al. Interleukin-13 Activates Distinct Cellular Pathways Leading to Ductular Reaction, Steatosis, and Fibrosis. Immunity 2016; 45(1): 145-58.
40. Hart KM, Fabre T, Sciurba JC, et al. Type 2 immunity is protective in metabolic disease but exacerbates NAFLD collaboratively with TGF-beta. Sci Transl Med 2017; 9(396).
41. de Ruiter K, Tahapary DL, Sartono E, et al. Helminths, hygiene hypothesis and type 2 diabetes. Parasite immunology 2017; 39(5).
42. Morton GJ, Meek TH, Schwartz MW. Neurobiology of food intake in health and disease. Nat Rev Neurosci 2014; 15(6): 367-78.
43. Li Z, Yi CX, Katiraei S, et al. Butyrate reduces appetite and activates brown adipose tissue via the gut-brain neural circuit. Gut 2018; 67(7): 1269-79.

SUPPLEMENTAL DATA

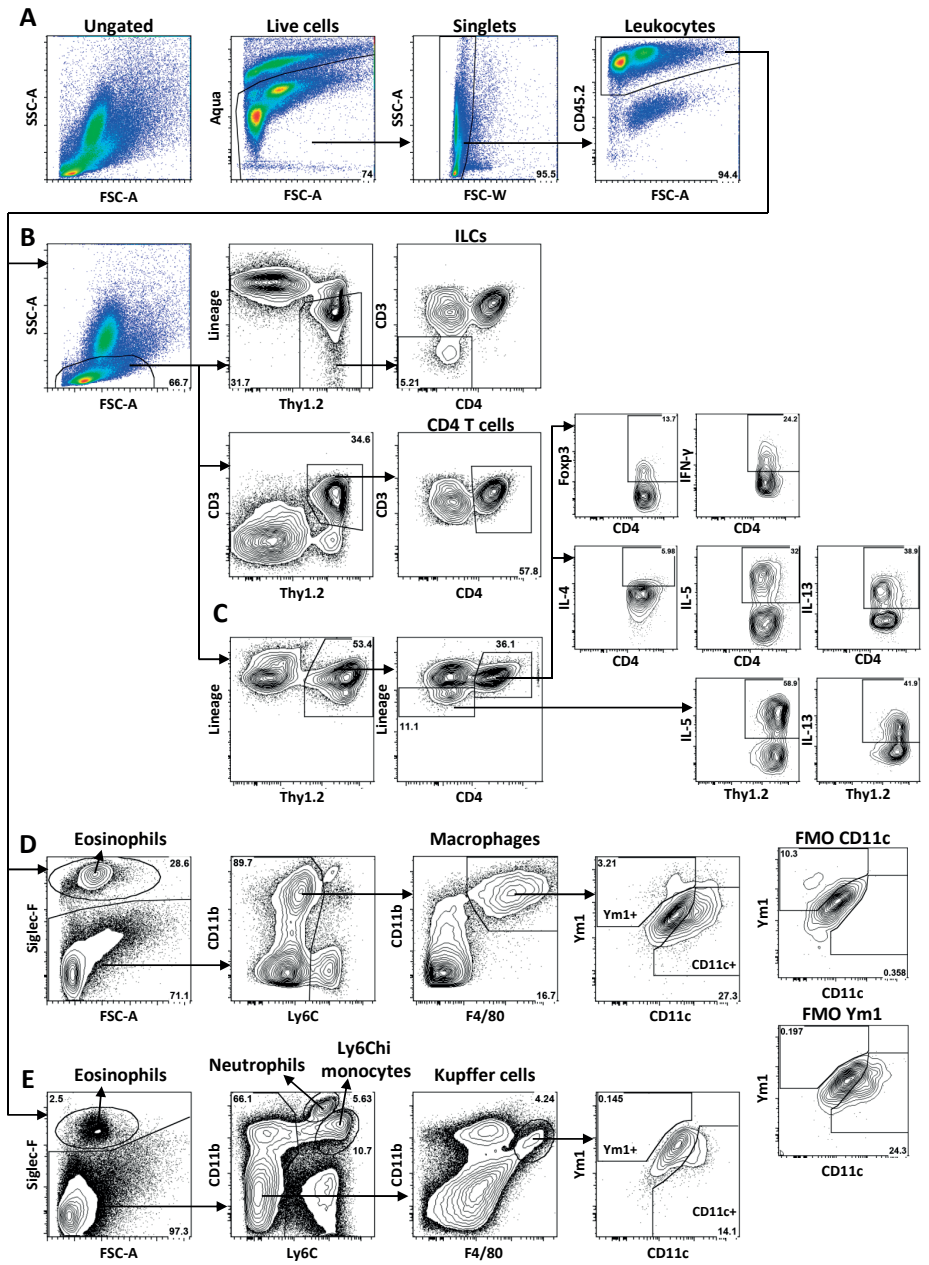

Supplementary Figure S1. Gating strategies. Isolated cells were pre-gated on Aqua$^-$CD45$^+$ single cells (*A*). The gating strategy for analysis of ILCs, CD4 T cells (*B*), CD4 T helper subsets and intracellular cytokine expression (*C*) is shown. Here, the lineage channel includes antibodies against CD11b, CD11c, B220, GR-1, NK1.1 and CD3. Representative samples were chosen from eWAT samples; gating strategies for lymphocyte subsets were similar in liver samples. The gating strategy is shown for eosinophils, CD11c$^+$Ym1$^-$ M1-like macrophages and CD11c$^-$Ym1$^+$ M2-like macrophages in eWAT, including Fluorescence Minus One (FMO) controls for CD11c and Ym1 (*D*). The gating strategy for liver eosinophils, neutrophils, Ly6Chi monocytes, CD11c$^+$Ym1$^-$ Kupffer cells and CD11c$^-$Ym1$^+$ Kupffer cells is shown (*E*).

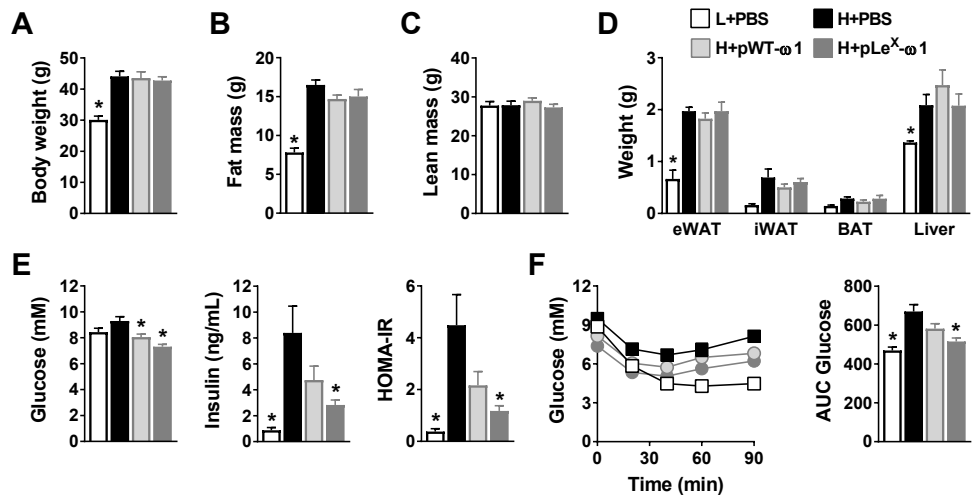

Supplementary Figure S2. ω1 glycovariants improve whole-body insulin sensitivity after one week of treatment, without affecting body composition. Mice were fed a LFD or a HFD for 12 weeks, after which they were treated i.p. with PBS or 50 µg pWT/pLe^X-ω1 once every 2 days for 1 week. Body weight was monitored throughout the experimental period (*A*). Body composition (*B-C*) and weights of different fat pads and the liver (*D*) were measured after 1 week of treatment. Blood glucose and plasma insulin levels were determined and HOMA-IR was calculated as described in the legend of Figure 1 (*E*). An i.p. insulin tolerance test was performed as described in the legend of Figure 1 (*F*). Results are expressed as means ± SEM. * $P<0.05$ *vs* HFD (n = 4-9 animals per group in A-E).

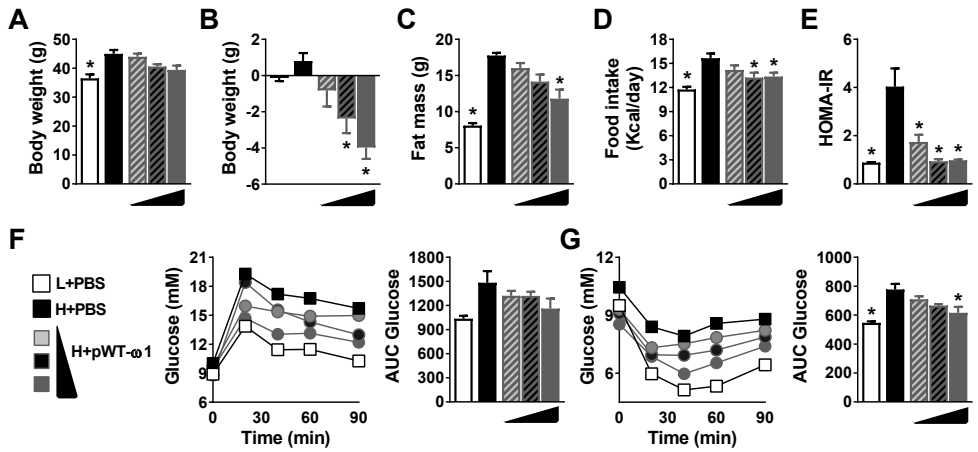

Supplementary Figure S3. pLe^{X}-ω1 improves whole-body insulin sensitivity and glucose tolerance in a dose-dependent manner. Mice were fed a LFD or a HFD and were treated i.p. with PBS or 10 µg, 25 µg or 50 µg pLe^{X}-ω1 every three days for four weeks. Body weight (*A-B*) and body composition (*C*) were determined after four weeks of treatment. Food intake was monitored throughout the treatment period (*D*). Blood glucose (*E*) and plasma insulin levels (*F*) were determined and HOMA-IR (*G*) was calculated as described in the legend of Figure 1. An i.p. glucose tolerance test (2 g/kg body weight; *H-I*) and i.p. insulin tolerance test (1U/kg lean body mass; *J*) were performed as described in the legend of Figure 1. Results are expressed as means ± SEM. * *P*<0.05 *vs* HFD (n = 3-4 animals per group).

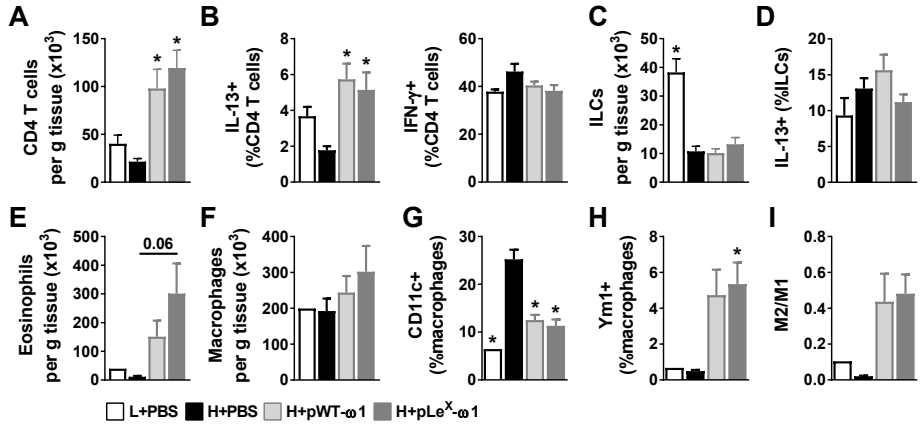

Supplementary Figure S4. ω1 glycovariants increase WAT type 2 immune cells after one week of treatment. Mice were fed a LFD or a HFD and treated with PBS or pWT/pLe^{X}-ω1 as described in the legend of Figure S2. At the end of the experiment, eWAT was collected, processed and analyzed as described in the legend of Figure 2. The numbers per gram tissue of CD4 T cells (*A*) and the frequencies of intracellular cytokine producing CD4 T cells (*B*) were determined. Numbers per gram tissue of ILCs were assessed (*J*), and frequencies of intracellular cytokine producing ILCs were determined (*D*). Cell numbers per gram tissue of eosinophils (*E*) and macrophages (*F*), and percentages of CD11c^{+}Ym1^{-} (M1-like; *G*) and CD11c^{-}Ym1^{+} (M2-like; *H*) in macrophages were determined. The M2 over M1 ratios were calculated (*I*). Results are expressed as means ± SEM. * *P*<0.05 *vs* HFD (n = 1-6 animals per group).

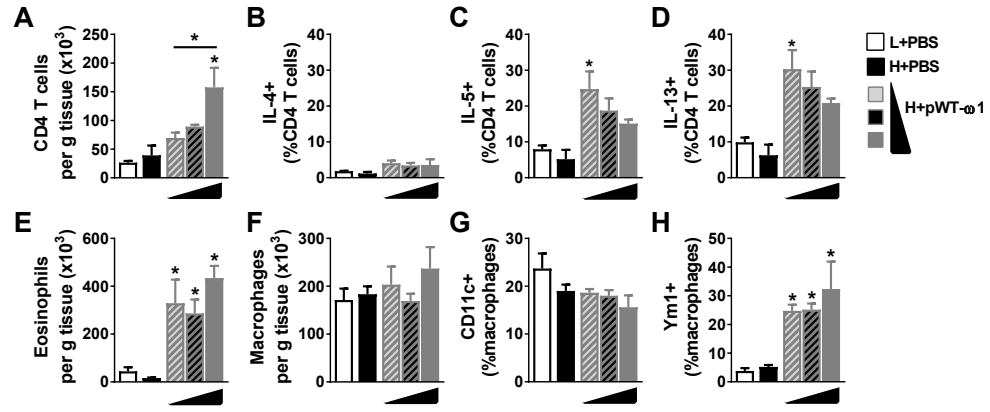

Supplementary Figure S5. pLe^{X}-ω1 increases WAT type 2 immune cells in a dose-dependent manner. Mice were fed a LFD or a HFD and were treated with PBS or pLe^{X}-ω1 as described in the legend of Figure S3. At the end of the experiment, eWAT was collected, processed and analysed as described in the legend of Figure 2. The numbers per gram tissue of CD4 T cells (*E*), and the frequencies of intracellular cytokine producing CD4 T cells (*B-D*) were determined. Numbers per gram tissue of eosinophils (*E*) and macrophages (*F*), and macrophages phenotypes (*G-H*) were assessed. Results are expressed as means ± SEM. * *P*<0.05 *vs* HFD or as indicated (n = 3-4 animals per group).

Supplementary table S1. Primer sequences for qRT-PCR

Gene	Accession number	Forward primer	Reverse primer
Acta2	NM_007392.3	AGCCATCTTTCATTGGGATGG	CCCCTGACAGGACGTTGTTA
Ccl2	NM_011333.3	TCAGCCAGATGCAGTTAACGCCC	GCTTCTTTGGGACACCTGCTGCT
Cidea	NM_007702	CTCGGCTGTCTCAATGTCAA	CCGCATAGACCAGGAACTGT
Col1a1	NM_007742.3	GAGAGGTGAACAAGGTCCCG	AAACCTCTCTCGCCTCTTGC
Cox8b	NM_007751.3	GACCCCGAGAATCATGCCAA	CCTGCTCCACGGCGGAA
Il1b	NM_008361	GACCCCAAAAGATGAAGGGCT	ATGTGCTGCTGCGAGATTTG
Rplp0	NM_007475	TCTGGAGGGTGTCCGCAACG	GCCAGGACGCGCTTGTACCC
Tgfb1	NM_011577	GCTGAACCAAGGAGACGGAA	ATGTCATGGATGGTGCCCAG
Timp1	NM_001044384	TCGGACCTGGTCATAAGGGC	GCTTTCCATGACTGGGGTGT
Tnfa	NM_013693	GTCCCCAAAGGGATGAGAAG	CACTTGGTGGTTTGCTACGA
Ucp1	NM_009463	TCAGGATTGGCCTCTACGAC	TGCATTCTGACCTTCACGAC
Zfp423	NM_033327.2	TTCACAGTCTTCGTCCAGGC	AGATTTTGTCCTCCTGCCCG